Journal of Solid State Chemistry **155,** 29–36 (2000)
doi:10.1006/jssc.2000.8881, available online at http://www.idealibrary.com on IDEAL®

Mixed Valent Gold Oxides: Syntheses, Structures, and Properties of $Rb_5Au_3O_2$, $Rb_7Au_5O_2$, and $Cs_7Au_5O_2$

Anja-Verena Mudring, Jürgen Nuss, Ulrich Wedig, and Martin Jansen[1]

Max-Planck-Institut für Festkörperforschung, Heisenbergstrasse 1, D-70569 Stuttgart, Germany

Received June 2, 2000; in revised form July 11, 2000; accepted July 17, 2000

DEDICATED TO PROFESSOR J. M. HONIG

The title compounds $Rb_5Au_3O_2$, $Rb_7Au_5O_2$, and $Cs_7Au_5O_2$ are the first examples of mixed valent phases containing gold in the oxidation states +1 and −1. Their crystal structures ($Rb_5Au_3O_2$, *Pbam*, $a = 736.4(1)$ pm, $b = 1430.8(2)$ pm, $c = 567.9(1)$ pm, $Z = 2$, $R(F) = 0.053$, 647 reflections; $Rb_7Au_5O_2$, *Immm*, $a = 567.1(2)$ pm, $b = 930.1(1)$ pm, $C = 1659.4(3)$ pm, $Z = 2$, $R(F) = 0.066$, 409 reflections; $Cs_7Au_5O_2$, *Immm*, $a = 599.4(1)$ pm, $b = 960.6(3)$ pm, $c = 1720.8(12)$ pm, $Z = 2$, $R(F) = 0.039$, 386 reflections) are characterized by the combination of distinctive structural features of gold(I) oxides and aurides: for Au(+1) a typical linear coordination by oxygen is found and the surroundings of Au(−1) bear a close resemblance to the binary 1:1 aurides. In consequence the overall structures of $Rb_5Au_3O_2$ and $M_7Au_5O_2$ can be described as intergrowths of M_3AuO_2 and MAu (M = Rb, Cs), constituting members of a homologous series $[MAu]_n[M_3AuO_2]$ with $n = 2$ and 4, respectively. The crystal chemical evidence for the valence states assumed, also confirmed by Mößbauer spectroscopy, is supported by various band structure calculations (Hartee–Fock and density functional) clearly indicating the coexistence of two different oxidation states. The compounds have been synthesized by reacting binary aurides MAu and alkali monoxides M_2O (M = Rb, Cs) with elemental gold in the required stochiometric amounts. Hereby, a further astonishing parallel to the chemistry of halogens is revealed. Like these, gold disproportionates upon interaction with bases. © 2000 Academic Press

Key Words: **mixed valency; gold chemistry; aurates; aurides; solid state reactions; intergrowth; band structure calculation.**

INTRODUCTION

As a basic principle in chemistry, in a given solid atoms of the same type strive for identical valence states and geometric surroundings. Violations of this rule, which are admittedly quite numerous, usually feature interesting physical and structural phenomena. During the past years, charge, spin, and orbital ordering have attracted increasing attention (1) because such collective processes seem to be strongly related to the occurrence of, e.g., superconductivity or magneto resistance. Prerequisities are mixed valency and markedly correlated electrons. The crucial balance between disordering and ordering of charge is controlled by intrinsic properties (e.g., ionization potentials) of the respective element and the structural changes that favor certain valence states. In mixed valent compounds containing transition metals, or main group elements, the formal charges of the single atoms usually differ by one or by two units of the same absolute sign, respectively. Solids containing both an element in a positive and negative oxidation state are extremely rare. Examples are ammonium nitrite and the alkalides of the general formula $A^-[A^+\text{crypt}]$ (2). This latter type of mixed valency is stabilized by a positive electron affinity of the respective element, and by the complexation of the positively charged species.

Here we report on the disproportionation of elemental gold in the presence of a heavy alkalimetal and its monoxide, resulting in crystalline ternary oxides in which well-defined Au(− 1) and Au(+ 1) coexist.

EXPERIMENTAL

Preparation. Feasible accesses to the mixed auride aurates mentioned are both solid state reaction of the binary auride, the alkali monoxide and elemental gold, and reaction of a mixture of alkali monoxide, gold and alkaline metal in excess. For the solid state reaction the required amounts of MAu, M_2O (M = Rb, Cs), and gold are mixed in a dry box (M. Braun, Garching, Argon, $O_2 < 0.2$ ppm, $H_2O <$ 0.05 ppm), ground with a mortar and pestle, and filled into a gold container. The sealed reaction vessel is placed in a closed Duran glass tube and heated under argon at 425°C for one day. Samples of higher crystallinity are obtained when using an excess of alkali metal. Here, in a first step the monoxide is dissolved in the molten alkali metal, then gold is added, and the reaction mixture is heated at 200°C for two

[1]To whom correspondence should be addressed. E-mail: martin@jansen.mpi-stuttgart.mpg.de.

0022-4596/00 $35.00

weeks. Afterward the surplus alkali metal is removed by distillation in dynamic vacuum (10^{-3} mbar).

The binary aurides MAu (M = Rb, Cs) are obtained by melting together gold and a surplus of alkali metal in a glass tube. After heat treatment at 200°C for several days, the unreacted alkali metal is distilled off in dynamic vacuum (10^{-3} mbar). The alkali metals themselves are prepared by reducing the corresponding chlorides with calcium (3), and are distilled twice before usage. The alkali monoxides are made by oxidizing the respective alkali metal with the appropriate amount of oxygen. In order to gain a homogeneous solid, the sample is reground, and annealed at 120°C (4). All these manipulations were carried out in Duran glass reaction vessels under Argon, freed from impurities by silica gel, molecular sieves, phosphoruspentoxide, and hot titanium sponge (900 K).

Elemental gold was precipitated by reducing tetrachloric gold acid with sodium oxalate (5).

X-ray diffraction. For x-ray crystal diffraction, single crystals were selected in a dry box (M. Braun, Garching, Germany) and mounted in sealed glass capillaries. Single-crystal intensity data for $Rb_7Au_5O_2$ and $Cs_7Au_5O_2$ were collected at room temperature either by using a four-circle diffractometer (Enraf–Nonius CAD4) with graphite-monochromatized Mo$K\alpha$ radiation and a scintillation counter with pulse height discrimination, or in the case of $Rb_5Au_3O_2$ on a Smart CCD 1000 area-detector diffractometer (Bruker AXS, Madison, WI). All relevant information concerning the data collection and structure refinement are given in Table 1. Atomic coordinates and thermal vibration parameters are listed in Table 2. The results of single-crystal structure analysis are confirmed by X-ray powder data (samples in sealed capillaries of diameter 0.3 mm; STADI P, Stoe, Darmstadt, Germany; linear position sensitive detector; Cu$K\alpha_1$ radiation, Silicon external standard). In contrast to the $M_7Au_5O_2$-type compounds, which are free from impurities, the powder pattern of $Rb_5Au_3O_2$ shows few unindexed lines of a minor unidentified phase.

Theoretical methods. To gain more insight into the valence states of Au, band-structure calculations have been performed on the experimental structures. Two different methods were employed in order to make sure that the interpretation of the results was not based on some artifacts originating from the computational approaches. Density

TABLE 1
Crystallographic Data and Structure Refinement

Empirical formula	$Rb_5Au_3O_2$	$Rb_7Au_5O_2$	$Cs_7Au_5O_2$
Formula weight [amu]	1050.25	1615.12	1947.2
Crystal size [mm]	$0.2 \times 0.2 \times 0.3$	$0.1 \times 0.1 \times 0.2$	$0.15 \times 0.15 \times 0.25$
Unit cell dimensions [pm]	$a = 736.4(1)$ $b = 1430.8(2)$ $c = 567.9(1)$	$a = 567.1(2)$ $b = 930.1(1)$ $c = 1659.4(3)$	$a = 599.4(1)$ $b = 960.6(3)$ $c = 1720.8(12)$
Space group (no.); Z	*Pbam* (55); 2	*Immm* (71); 2	*Immm* (71); 2
V [$cm^3 \cdot mol^{-1}$]; ρ_{Xray}[$g \cdot cm^{-3}$]	180.15(4); 5.830	263.6(1); 6.128	298.3(2); 6.527
Absorption coefficient [mm^{-1}]	56.85	49.54	61.07
Data collections and corrections	Bruker AXS Smart CCD 1000; Mo$K\alpha$ (λ = 71.073 pm); semi empirical absorption correction, SADABS[a]	Enraf–Nonius CAD4; Mo$K\alpha$ (λ = 71.073 pm); empirical absorption correction (ψ scans)	
θ range	$5° \le 2\theta \le 58°$	$5° \le 2\theta \le 54°$	$5° \le 2\theta \le 48°$
Structure solution and refinement	Direct methods, SHELXS-97[b]; full-matrix least- squares (F^2), SHELXTL-97[b]		
Variable parameters	34	30	30
N (hkl); N′ (hkl) with $I > 2\sigma(I)$	877; 647	581; 40.9	461; 386
$R(F)_N$; $R_w(F^2)_{N'}$	0.053; 0.073	0.066; 0.097	0.039; 0.052
$R_w(F^2)_N$; $R_w(F^2)_{N'}$	0.135; 0.129	0.186; 0.166	0.073; 0.067
Extinction coefficient	0.0064(6)	0.0006(2)	0.0012(1)
ΔF_{max}; ΔF_{min} [$e \cdot Å^{-3}$]	5.7; −2.7	4.1; −4.4	3.2; −1.7
Weighting w	$q_1 = 0.035$; $q_2 = 0$	$q_1 = 0.101$; $q_2 = 38.95$	$q_1 = 0$; $q_2 = 7.59$

Note.

$$R_w(F^2) = \sqrt{\frac{\sum w(F_o^2 - F_c^2)^2}{\sum w(F_o^2)^2}}; \quad R(F) = \frac{\sum \|F_o| - |F_c\|}{\sum |F_o|}$$

$w^{-1} = [\sigma^2(F_o^2) + q_1 \cdot P^2 + q_2 \cdot P]$ with $P = \frac{1}{3}(F_o^2 + 2F_c^2)$.

[a]SADABS: G. M. Sheldrick, Bruker AXS, Inc. Madison, WI (1998).
[b]SHELXS, SHELXTL: G. M. Sheldrick, Bruker AXS, Inc. Madison WI, SHELXTL Version 5.1 (1997).

TABLE 2
Atomic Parameters and Thermal Vibration Parameters U_{ij} [pm^2] (Standard Deviations)

Compound	Atom	Site	x	y	z	U_{eq}	U_{11}	U_{22}	U_{33}	U_{12}	U_{13}	U_{23}
$Rb_5Au_3O_2$	Au1	2*a*	0	0	0	186(3)	165(6)	138(6)	257(5)	10(5)	0	0
	Au2	4*h*	0.3511(2)	0.1440(1)	$\frac{1}{2}$	402(4)	393(7)	359(7)	453(6)	55(5)	0	0
	Rb1	2*c*	0	$\frac{1}{2}$	0	346(6)	276(19)	283(18)	479(15)	90(15)	0	0
	Rb2	4*g*	0.1128(4)	0.2360(2)	0	341(6)	247(14)	253(12)	524(11)	−82(10)	0	0
	Rb3	4*h*	0.3297(4)	0.3972(2)	$\frac{1}{2}$	338(6)	403(16)	361(15)	251(8)	−71(11)	0	0
	O1	4*g*	0.329(2)	0.391(1)	0	231(32)	143(84)	135(77)	414(68)	−73(60)	0	0
$Rb_7Au_5O_2$	Au1	2*a*	0	0	0	230(6)	304(12)	231(11)	156(8)	0	0	0
	Au2	4*i*	0	0	0.3482(1)	590(8)	883(18)	452(14)	437(10)	0	0	0
	Au3	4*j*	$\frac{1}{2}$	0	0.1929(2)	574(8)	626(17)	424(14)	673(14)	0	0	0
	Rb1	2*d*	$\frac{1}{2}$	0	$\frac{1}{2}$	524(18)	643(51)	252(33)	677(42)	0	0	0
	Rb2	4*h*	0	0.2888(6)	$\frac{1}{2}$	383(10)	349(23)	380(25)	420(19)	0	0	0
	Rb3	8*l*	0	0.2219(4)	0.1661(1)	410(8)	544(21)	463(19)	223(11)	0	0	−41(12)
	O1	4*g*	0	0.216(3)	0	268(56)	270(150)	87(100)	450(130)	0	0	0
$Cs_7Au_5O_2$	Au1	2*a*	0	0	0	179(5)	197(8)	166(9)	175(9)	0	0	0
	Au2	4*i*	0	0	0.3531(1)	555(6)	776(10)	463(11)	427(11)	0	0	0
	Au3	4*j*	$\frac{1}{2}$	0	0.1875(1)	496(6)	512(9)	389(10)	587(12)	0	0	0
	Cs1	2*d*	$\frac{1}{2}$	0	$\frac{1}{2}$	441(9)	508(15)	170(13)	645(24)	0	0	0
	Cs2	4*h*	0	0.2908(2)	$\frac{1}{2}$	330(6)	211(8)	364(12)	413(14)	0	0	0
	Cs3	8*l*	0	0.2196(2)	0.1685(1)	353(5)	427(8)	401(9)	231(9)	0	0	−42(6)
	O1	4*g*	0	0.210(1)	0	218(39)	218(88)	201(83)	236(108)	0	0	0

functional calculations have been carried out within the TB-LMTO-ASA formalism (tight-binding linear muffin tin orbitals atomic sphere approximation (6)), using the local exchange correlation functional of Barth and Hedin (7). For the Hartree–Fock calculations, the CRYSTAL98 program package (8) was applied.

For both methods it is important to carefully analyze the parameters that define the basis sets. Problems arose due to the fact that there are two very different environments for the gold atoms in the compounds, the relatively compact $[AuO_2]^{3-}$ dumbbells and the more open gold alkali metal partial structures.

The atomic sphere approximation within the LMTO program requires a complete filling of space by atomic muffin tin spheres. Thus, the spheres must overlap. To compensate for the error introduced by the overlap, corrections (9) are included in the program, which are valid up to a certain amount of overlap. To reduce the overlap, empty spheres can be introduced. Applying the default criteria for an empty spheres search, the program finds 11 classes of empty spheres, due to the structural features mentioned above. This drastically increases the number of basis functions, and leads to convergence problems ($Rb_7Au_5O_2$), as well as to small, but significant fluctuations in the electron density and in the electron localization function (ELF). In the case of $Rb_5Au_3O_2$ this leads to difficulties in defining ELF basins. After increasing the maximum allowed overlap o slightly ($o = 0.164$ instead of $o = 0.16$), only one class of empty spheres was necessary. The band structure is practically not affected by this slightly higher tolerance value. Therefore, $o = 0.164$ was used for all calculations. With the one class of empty spheres, the atomic radii in $Rb_5Au_3O_2$ were (in a.u.) Au1, 2.53; Au2, 3.96; Rb1, 4.12; Rb2, 3.93; Rb3, 3.90; O1, 1.86.

The choice of an appropriate Gaussian basis set for the Hartree–Fock CRYSTAL98 calculations was difficult in two respects. First, the basis set must describe all gold atoms (see above) as consistently as possible. The idea of using two different basis sets for gold atoms in different crystallographic locations was rejected in order not to prejudice the results. The second difficulty arose from the practical realization of the algorithms in the CRYSTAL98 program. "The risks of numerical catastrophes increase rapidly with a decreasing exponent" (cited from (8)). The basis set chosen allows a compromise between accuracy and numerical stability of the calculation. For Au we used a 19-valence-electron pseudopotential (10a, b). The original basis was reduced to [5*s* 4*p* 2*d*] by omitting 2*s*, 1*p*, and 1*d* functions with the most diffuse exponents. For $Rb_7Au_5O_2$ even another *p* function had to be taken away as it lead to numerical instabilities, even when varying the exponent. The 9-valence-electron pseudopotential for Rb was taken from Ref. (11). The corresponding basis (12) was reduced to [3*s* 3*p*] by omitting the most diffuse functions. Finally, we used a 6-valence-electron pseudo-potential for oxygen (13). The exponent of the outermost *p* function of the original basis was increased ($\eta = 0.15$) to obtain numerical stability. The addition of a third *s* function lead to convergence problems with $Rb_5Au_3O_2$ over a wide range of exponents.

To describe the electronic structure of compounds including heavy elements properly, relativistic effects must be taken into account. This was done with the LMTO program by using the radial one-particle Dirac equation to determine the partial waves within the muffin tin spheres. In the Hartree–Fock calculation the relativistic effects of the core electron were included in the pseudo-potentials through an appropriate adjustment.

In addition to the analysis of the band structure, the ELF (14, 15) was calculated from the LMTO wave function in order to gain insight into the bonding properties. By the topological analyses of the ELF (16) and the integration of the charge density within the ELF basins, the charge distribution within the crystals was determined. Complementary, the bonding properties of the $[AuO_2]^{3-}$ dumbbells were analyzed by calculating the Crystal Orbital Hamilton Population (COHP) (17). The charge distributions from the Hartree–Fock wave functions were obtained by a Mulliken population analysis.

RESULTS AND DISCUSSION

The novel ternary oxides $Rb_5Au_3O_2$, $Rb_7Au_5O_2$, and $Cs_7Au_5O_2$ contain gold as anionic Au(−1) and cationic Au(+1) species, at the same time. This can be deduced rather conclusively from their structral features, already. Au(+1) is coordinated linearly by oxygen at an average distance (cf. Table 3) of 201 pm, which is typical for gold in such a valence state (18), while those gold atoms to which we assign a negative oxidation state are solely surrounded by alkali metal atoms with distances ranging from $d_{(Au-Rb)} = 348.9$ to 388.4 pm and $d_{(Au-Cs)} = 366.0$ to 404.7 pm (Table 3). Looking closer at the structures their first coordination shells are virtually identical to those found in the corresponding binary aurides CsAu and RbAu (19, 20). Amazingly, this situation is stable with respect to internal redox processes which would level out the opposite charges. The aurate(+1) and auride(−1) parts are distinctly separated from each other. Figure 1 shows the stackings of layers of composition RbAu and Rb_3AuO_2, constituting $Rb_5Au_3O_2$ and $Rb_7Au_5O_2$, respectively. Thus, both structures can be understood as intergrowths (21) of an alkali metal aurate and a respective alkali metal auride, constituting members of a still fragmentary homologous sequence $[RbAu]_n[Rb_3AuO_2]$ with $n = 2$ and 4. However, the structure plots in Fig. 1 are overemphasizing this view somewhat, since the separations between Au^- and the alkali metal atoms are in the same range for the interlayer and intralayer contacts.

TABLE 3
Distances [pm] (Standard Deviations)

$Rb_5Au_3O_2$	Distance	Mult.	$Rb_7Au_5O_2$	Distance	Mult.	$Cs_7Au_5O_2$	Distance	Mult.
Au1–O1	200(1)	2	Au1–O1	201(3)	2	Au1–O1	202(1)	2
–Rb1	368.2(1)	2	–Rb2	345.0(3)	4	–Cs2	360.8(1)	4
–Rb2	347.7(3)	2	–Rb3	344.3(3)	4	–Cs3	358.6(2)	4
–Rb3	343.5(2)	4						
			Au2–Rb1	379.3(2)	2	Au2–Cs1	392.1(2)	2
Au2–Rb1	367.6(1)	2	–Rb2	368.3(4)	2	–Cs2	376.8(2)	2
–Rb2	358.8(2)	2	–Rb3	366.0(3)	2	–Cs3	381.3(3)	2
	383.7(2)	2		384.6(3)	4		404.7(1)	4
–Rb3	357.4(3)	1						
	362.6(3)	1	Au3–Rb2	375.6(4)	2	Au3–Cs2	380.1(2)	2
	383.7(2)	1	–Rb3	348.9(3)	2	–Cs3	366.0(2)	2
	388.4(3)	1		353.5(2)	4		367.9(1)	4
Rb1–O1	288(1)	2	Rb1–O1	264(3)	2	Cs1–O1	278(1)	2
–Au2	367.5(1)	4	–Au2	379.3(2)	4	–Au2	392.1(2)	4
Rb2–O1	274(1)	2	Rb2–O1	283.6(1)	2	Cs2–O1	299.7(1)	2
–Au2	358.8(2)	2	–Au2	368.3(4)	2	–Au2	376.8(2)	2
	383.7(2)	2	–Au3	375.6(4)	2	–Au3	380.1(2)	2
Rb3–O1	284.1(1)	2	Rb3–O1	275.6(2)	1	Cs3–O1	290.1(2)	1
–Au2	357.4(3)	1	–Au2	366.0(3)	1	–Au2	381.3(3)	1
	362.6(3)	1		384.6(3)	2		404.7(1)	2
	377.5(3)	1	–Au3	348.9(3)	1	–Au3	366.0(2)	1
	388.4(3)	1		353.5(2)	2		367.9(1)	2
O1–Au1	200(1)	1	O1–Au1	201(3)	1	O1–Au1	202(1)	1
–Rb1	288(1)	1	–Rb1	264(3)	1	–Cs1	278(1)	1
–Rb2	274(1)	2	–Rb2	283.6(1)	2	–Cs2	299.7(1)	2
–Rb3	284.1(1)	2	–Rb3	275.6(2)	2	–Cs3	290.1(2)	2

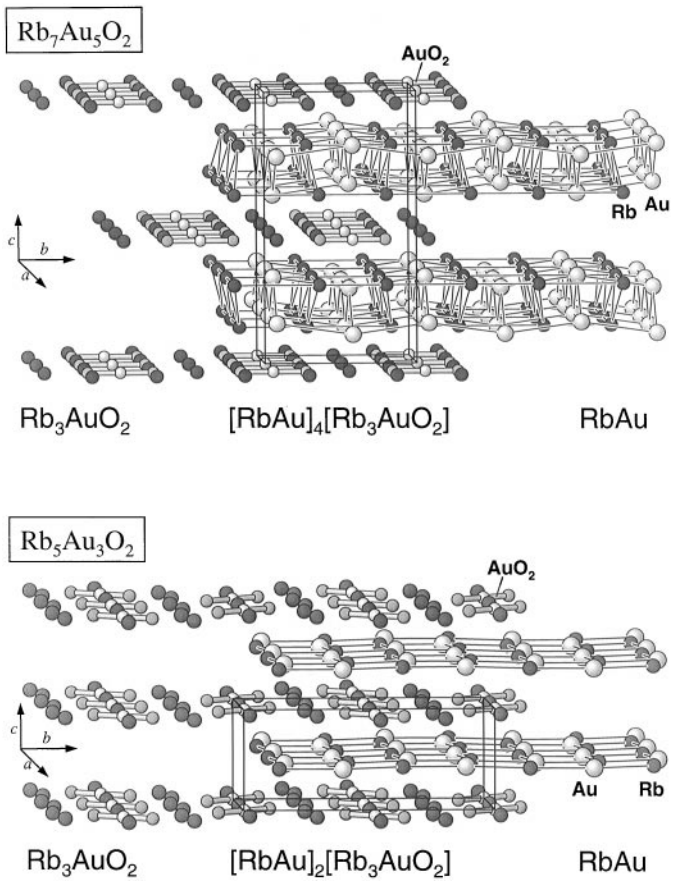

FIG. 1. $Rb_7Au_5O_2$ (top) and $Rb_5Au_3O_2$ structure (bottom) with unit cell.

An alternative description of the underlying structural principles becomes apparent when analyzing the arrangements of all the metal atoms only (22, 23). In both cases these are related to structure types occurring with metals or intermetallic phases. In this sense, the metal atom positions of $Rb_5Au_3O_2$ fully match the Rh_5Si_3 structure, while $Rb_7Au_5O_2$ and $Cs_7Au_5O_2$ are characterized by a cubic body centered arrangement. In the latter, the positions are occupied by alkali metals and gold prevailingly according to the β-brass-type structure, cf. Fig. 2. As is pointed out by the formula $A_6B_6 \equiv Rb_6(Au_5Rb)$, the B positions are shared in the ratio 5:1 by gold and rubidium. Cubic coordination polyhedra are also found in $Rb_5Au_3O_2$. However, the full framework is constituted from slabs of face-sharing cubes by chemical twinning (Fig. 2) (24). These intermetallic arrangements are stuffed with oxygen atoms, which in either case are located at opposite faces of the AuM_8 cubes (M = Rb, Cs).

$Rb_5Au_3O_2$ and $M_7Au_5O_2$ (M = Rb, Cs) are very beautiful examples how nature can form complex structures by combining simple building units. Regarding the three-dimensional arrangement of cubes it becomes apparent that the structure of $Rb_5Au_3O_2$ allows for a classification as *homogeneous intergrowth* (chemical twinning) (25) while in the case of $M_7Au_5O_2$ the structure is described best as *inhomogeneous intergrowth* (26). The former structure is built up by blocks of the same kind but with different orientations (*A A′ A*; cf. Fig. 2, bottom), the latter one by combining different building units in the same manner (*A B A B*; cf. Fig. 2, top).

The reactions by which the title compounds have formed add a completely novel aspect to the chemistry of gold. Obviously, gold, one of the most inert metals, readily disproportionates at the interaction of basic oxides:

$$3Rb + 5\mathbf{Au^{\pm 0}} + 2Rb_2O \longrightarrow [Rb\mathbf{Au^{-1}}]_4[Rb_3\mathbf{Au^{+1}}O_2] \quad [1]$$

$$\mathbf{Cl_2^{\pm 0}} + 2NaOH \longrightarrow Na\mathbf{Cl^{-1}} + Na\mathbf{Cl^{+1}}O + H_2O. \quad [2]$$

A driving force for this reaction seems to be the energy gained by complexation of Au(+1) by oxide ions in the solid state. Another contribution for stabilizing this unconventional valence situation can be seen in the high electron affinity of gold, which is comparable to that of iodine. This latter peculiarity of gold expresses itself at the formation of the auride anions in intermetallics like MAu (M = Rb, Cs) (19,20), or in perovskite-type ternary aurides M_3AuO (M = Rb, Cs) (27). Here, as we have demonstrated previously (28–30), gold exists as a well-defined singly charged anion in ionic crystals. The structural similarities of oxide halides and oxide aurides indicate another close relationship between the chemistry of gold and halogens (31).

The disproportionation of elemental gold, as described here, constitutes another amazing parallel to the chemistry of halogens, which also disproportionate when exposed to bases (liquid or solid), cf. Eq. [2]. The dark red rubidium compounds, and the orange cesium compound, are extremely sensitive toward the atmosphere. In water they decompose into elemental gold and Au(+3). The dark violet suspension of elemental gold turns to a yellow solution upon adding hydrochloric acid, because the tetrachloro complex of Au(+3) forms.

Our assignment of the oxidation states by crystal chemical evidence is supported by the results of Mößbauer spectroscopy, which clearly show two considerably different gold species to be present in the sample. The chemical shifts and the quadrupole splittings are indicative for $[AuO_2]^{3-}$ units and Au^-, respectively (32).

The results of the band structure calculations, too, unambiguously show the different character of the gold atoms. The band structure of $Rb_5Au_3O_2$ is presented in Fig. 3 within the "fatband" representation; e.g., the width of the lines is proportional to the projection onto some atomic orbitals. The Au2 (Au(−1)) *d* bands (Fig. 3a) are nearly

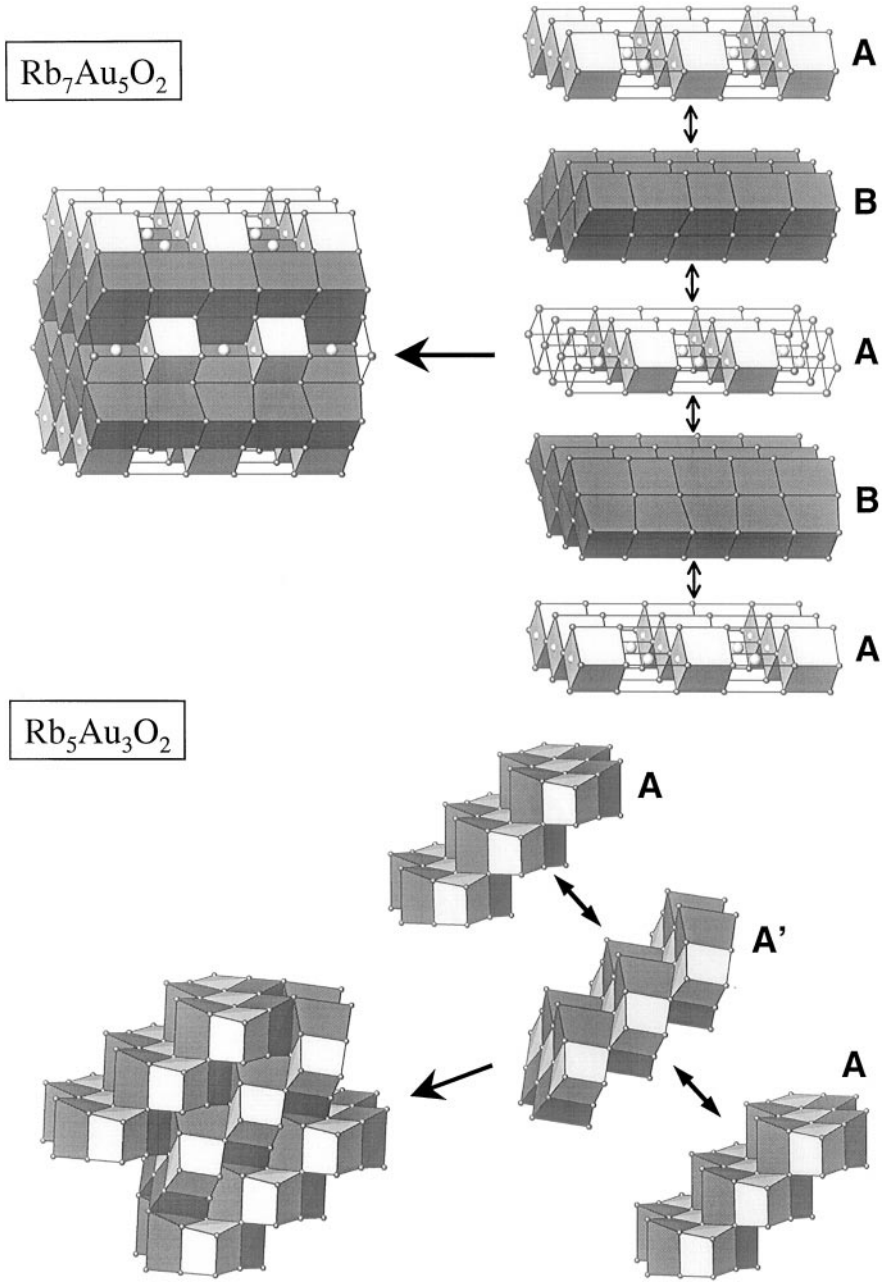

FIG. 2. Crystal structures of $Rb_7Au_5O_2$ (top) and $Rb_5Au_3O_2$ (bottom) emphasizing that both structures represent three-dimensional arrangements of cubes (white cubes = AuO_2Rb_8, dark cubes = $AuRb_8$, open cubes = $RbRb_8$). The principles of inhomogeneous and homogeneous intergrowth are pointed out.

degenerate with practically no dispersion, indicating a closed *d* shell. About 0.07 Ry above, there are bands with main contributions of the 6*s* orbitals of Au2 (Fig. 3b). The *d* bands of the gold atoms Au1 (Au(+ 1)) within the dumbbells also show little dispersion, but are split over the entire valence region. Between − 0.6 and − 0.5 Ry the bands have mainly *d* character, whereas the lowest and the highest valence bands have significant contributions from the oxygen *p* orbitals. The COHPs in these energy regions show that the lowest valence bands are bonding, whereas the highest ones are anti-bonding. The integration of COHP up to the Fermi level yields − 0.235 Ry/Au–O bond (note, COHP and COOP have opposite sign), indicating the low covalent character of the Au–O bond. This is confirmed by the Hartree–Fock overlap population which only gives 0.16 for the Au–O bond. In fact, the Hartree–Fock band structure shows the same characteristics as the LMTO band structure described above.

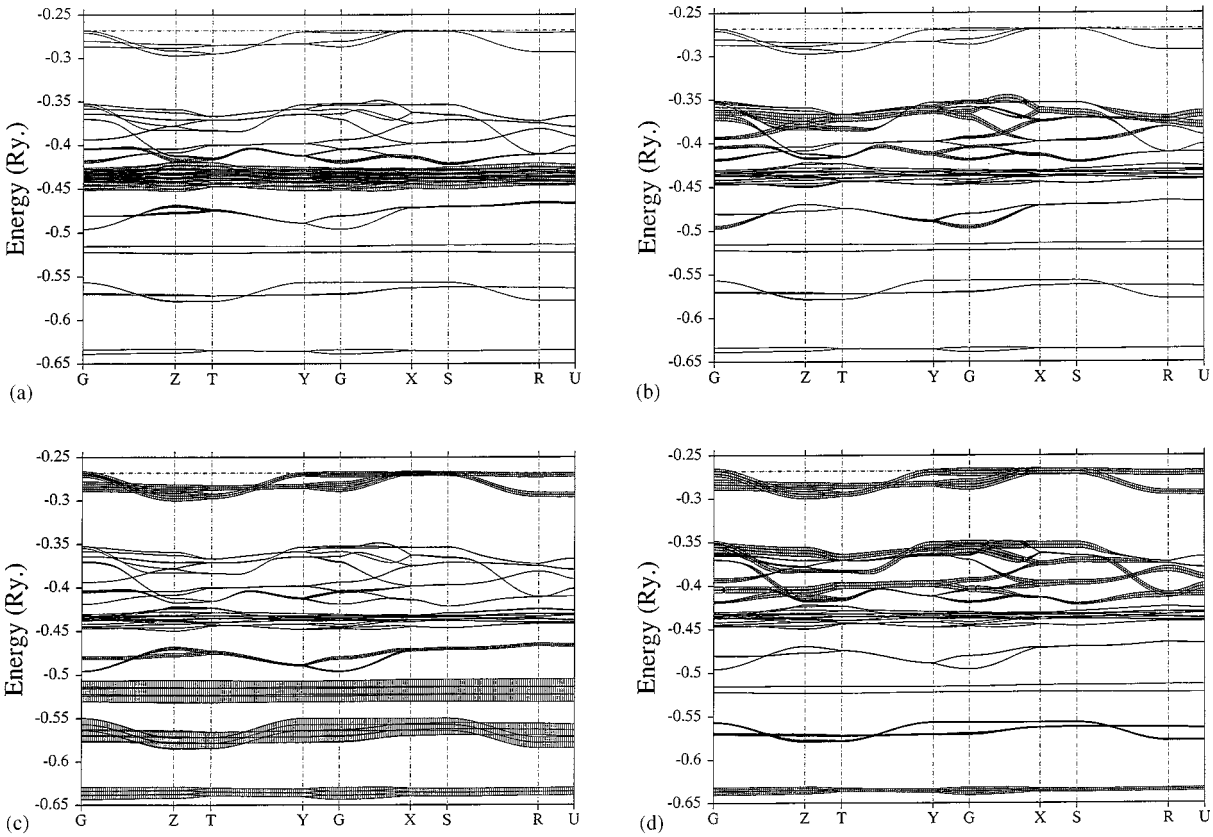

FIG. 3. The bandstructure of $Rb_5Au_3O_2$. The width of the "fatbands" is proportional to the specified orbital character: (a) Au2 5*d*, (b) Au2 6*s*, (c)Au1 5*d*, (d) O1 2*p*.

The domains within the isosurfaces of the ELF calculated for the valence bands for a value of 0.375 are represented in Fig. 4. The maximum of the ELF at the oxygen atoms forms a ring-type attractor with a value of 0.7. At ELF 0.44, attractors appear on the Au1–O bonds close to the oxygen atoms. The attractor at Au1 (ELF 0.43) is also a ring type as can be seen by the form of the domains in Fig. 4. This indicates that the *d* shell of the gold atoms within the dumbbells is not completely filled, which is consistent with the result of the population analysis which gives a *d* population of 9.7 for Au1. Below ELF = 0.2, the domains around the atoms of the dumbbells grow together to one single domain. The attractors attributed to the Au2 atoms appear at ELF 0.38. The corresponding domains are distorted spheres. No bifunctional can be seen above ELF = 0.07. This clearly demonstrates the exclusively ionic character of the Au2 atoms.

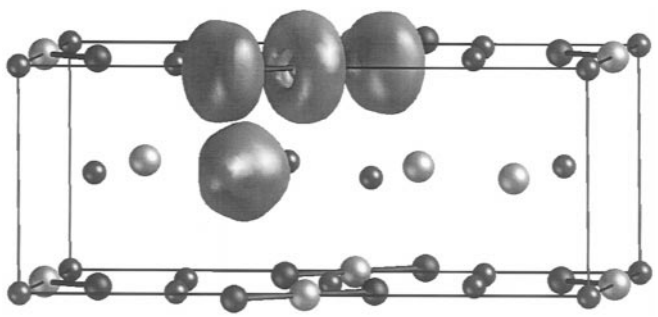

FIG. 4. Selected domains of the electron localization function (ELF = 0.375) in $Rb_5Au_3O_2$.

Applying a topological analysis of the ELF, one can determine zero-flux surfaces that separate the space into basins attributed to the individual attractor. After integrating electron density within these basins partial charges for these regions can be calculated (O, −0.99; Au1–O, −0.29; Au1, +0.10; Au2, −0.86). Whether the small basin belonging to the attractor on the Au1–O bond shows the covalent part of the bond or should be attributed to oxygen is not clear. Irrespectively, the low covalent character of the Au1–O band as discussed above is confirmed by the ELF. The net charges obtained from population analysis (O, −1.42; Au1, −0.05; Au2, −1.01; Rb, +0.98) are rather close to the values obtained from ELF. The electronic structure of $Rb_7Au_5O_2$ shows all the same features as those

of $Rb_5Au_3O_2$ discussed above. Thus all the conclusions also apply to $Rb_7Au_5O_2$.

Both density functional and Hartree–Fock calculations draw a consistent picture of the electronic structure. They prove that Au2 is a slightly polarized Au^- anion. The positive charge of Au1 is definitively smaller than expected by general considerations, and is distributed within the dumbbells over a rather wide space. This may be a further stabilizing factor for the coexistence of gold anions and cations in the investigated compounds.

ACKNOWLEDGMENTS

The authors acknowledge the Fonds der Chemischen Industrie for financial support. A.-V. Mudring thanks the Studienstiftung der Hoechst AG, the Fonds der Chemischen Industrie, the Dr. Wilhem Heinrich und Else Heraeus Stitfung, and the Ev. Studienwerk Villigst e.V. and its members for support.

REFERENCES

1. Y. Tokura and N. Nagaosa, *Science* **288,** 462 (2000).
2. J. Dye, R. H. Huang, and D. L. Ward, *J. Coord. Chem.* **18,** 121 (1988).
3. L. Hackspill, *C. R. Hebed. Séances Acad. Sci.* **154,** 209 (1912).
4. G. Brauer, "Handbuch der präparativen anorganischen Chemie," Vol. 2, p. 395. Enke, Stuttgart, 1975.
5. L. Vanino, "Handbuch der präparativen. Chemie," Vol. 1, p. 520. Enke, Stuttgart, 1921.
6. R. W. Tank, O. Jepsen, A. Burkhardt, and O. K. Andersen, TB-LMTO-ASA program, Version 4.7, Max-Planck-Institut für Festkörperforschung, Stuttgart, 1998.
7. W. Barth and L. Hedin, *J. Phys. C* **5,** 1629 (1972).
8. V. R. Saunders, R. Dovesi, C. Roetti, M. Causà, N. M. Harrison, R. Orlando, and C. M. Zicovich-Wilson, CRYSTAL98 User's Manual, University of Torino, Torino, 1998.
9. O. K. Andersen, Z. Pawlowska, and O. Jepsen, *Phys. Rev. B*: *Condens. Matter* **34,** 5253 (1986).
10. (a) D. Andrae, U. Haeussermann, M. Dolg, H. Stoll, at H. Preuss, *Theoret. Chim. Acta* **77,** 123 (1990); (b) All pseudopotential parameters, basis exponents, and contraction coefficients can be found on the Internet: http://www/theochem.uni-stuttgart.de.
11. T. Leininger, A. Nicklass, W. Küchle, H. Stoll, M. Dolg, and A. Bergner, *Chem. Phys. Lett.* **255,** 274 (1996).
12. A. Bergner, Arbeitsbericht 1990, Institut für theoretische Chemie, Universität Stuttgart
13. A. Bergner, M. Dolg, W. Kuechle, H. Stoll, and H. Preuss, *Mol. Phys.* **80,** 1431 (1993).
14. A. Savin, A. D. Becke, J. Flad, R. Nesper, H. Preuss, and H. G. von Schnering, *Angew. Chem.* **103,** 421 (1991); *Angew. Chem. Int. Ed. Engl.* **30,** 409 (1991).
15. A. Savin, O. Jepsen, J. Flad, O. K. Andersen, H. Preuss, and H. G. von Schnering, *Angew. Chem.* **104,** 186 (1992); *Angew. Chem. Int. Ed. Engl.* **31,** 187 (1992).
16. B. Silvi and A. Savin, *Nature* **371,** 683 (1994).
17. R. Dronskowski and P. E. Blöchl, *J. Phys. Chem.* **97,** 8617 (1993).
18. M. Jansen, A.-V. Mudring, *in* "Gold—Progress in Chemistry, Biochemistry and Technology" H. Schmidbaur, Ed., p. 745. Wiley, Chichester, 1999.
19. A. Sommer, *Nature* **215,** 3841 (1943).
20. W. E. Spicer, A. H. Sommer, and J. G. White, *Phys. Rev.* **115,** 57 (1959).
21. E. Parthé and B. Chabot, *in* "Handbook on the Physics and Chemistry of Rare Earth" (K. A. Gschneider and L. Eyring, Eds.), p. 113. Elsevier, Amsterdam, 1985.
22. M. O'Keefe and B. G. Hyde, *in* "Structure and Bonding," Vol. 61, p. 77. Springer-Verlag, Berlin, 1985.
23. A Vegas, *Cryst. Rev.* **7,** 189 (1999).
24. S. Andersson, *Angew. Chem.* **95,** 67 (1983); *Angew. Chem. Int. Ed. Engl.* **22,** 69 (1983).
25. P. I. Kripyakevich and Yu. N. Grin, *Sov. Phys. Crystallogr.* **23,** 45 (1978).
26. Yu. N. Grin, Ya. P. Yarmolyuk, and E. I. Gladyshevskii, *Sov. Phys. Crystallogr.* **27,** 413 (1982).
27. C. Feldmann and M. Jansen, *Z. Anorg. Allg. Chem.* **621,** 201 (1995).
28. C. Feldmann and M. Jansen, *Angew. Chem.* **105,** 1107 (1993); *Angew. Chem. Int. Ed. Engl.* **32,** 1049 (1993).
29. C. Feldmann and M. Jansen, *J. Chem. Soc. Chem. Commun.* 1045 (1994).
30. A. Pantelouris, G. Küper, J. Hormes, C. Feldmann, and M. Jansen, *J. Am. Chem. Soc.* **117,** 11,749 (1995).
31. C. Feldmann and M. Jansen, *Z. Anorg. Allg. Chem.* **621,** 1907 (1995).
32. F. E. Wagner, A.-V. Mudring, and M. Jansen, unpublished. $Rb_7Au_5O_2$: IS = 6.09(1) mms^{-1} (Au(−1)), IS = 3.94(1) mms^{-1}, QS = 7.24(1) mms^{-1} (Au(+1)); $Cs_7Au_5O_2$: IS = 7.44(1) mms^{-1} (Au(−1)), IS = 3.33(1) mms^{-1}, QS = 6.71(1) mms^{-1} (Au(+1)).